Journal of Materials Science & Technology 102 (2022) 195–203

Contents lists available at ScienceDirect

Journal of Materials Science & Technology

journal homepage: www.elsevier.com/locate/jmst

The dynamic compressive properties of magnetorheological plastomers: enhanced magnetic-induced stresses by non-magnetic particles

Haoming Pang[a,b], Zhenbang Xu[c], Longjiang Shen[d], Jun Li[b], Junshuo Zhang[a], Zhiyuan Li[b], Shouhu Xuan[a,*], Xinglong Gong[a,*]

[a] CAS Key Laboratory of Mechanical Behavior and Design of Materials, Department of Modern Mechanics, CAS Center for Excellence in Complex System Mechanics, University of Science and Technology of China (USTC), Hefei 230027, China
[b] Anhui Weiwei Rubber Parts Group Co. Ltd, Tongcheng 231400, China
[c] CAS Key Laboratory of On-orbit Manufacturing and Integration for Space Optics System, Changchun Institute of Optics, Fine Mechanics and Physics, Chinese Academy of Sciences, Changchun 130033, China
[d] Hunan Bogie Engineering Research Center, Zhuzhou 412000, China

ARTICLE INFO

Article history:
Received 16 March 2021
Revised 11 May 2021
Accepted 24 May 2021
Available online 27 August 2021

Key words:
Particle-reinforced composites
Stress/strain curves
Microstructures
Impact behavior
Mechanical properties

ABSTRACT

In this research, a series of hollow glass powder (HGP) reinforced magnetorheological plastomers (MRPs) were prepared to improve the impact resistance of the materials, and the dynamic compressive properties of MRPs under high strain rate were investigated by using a split Hopkinson pressure bar (SHPB) system equipped with a customized magnetic device. Experimental results showed the HGPs greatly enhanced the yield stresses of the MRPs. Especially, for MRPs with 9 vol.% carbonyl iron powders (CIPs), the magnetic-induced yield stress increased from 7.3 MPa to 17.1 MPa (134% increased) by adding 18 vol.% HGPs. The particle structures in MRPs were further simulated and the corresponding intergranular stress was calculated to study the enhancement effect of HGPs. The simulated results showed that more compact structures were formed with the excluded volume caused by secondary HGPs, so the yield stresses of the MRPs increased under a magnetic field. However, when the mass ratio of HGP to CIP was larger than 0.67, HGPs would hinder the formation of chain-like structures and reduce the magneto-mechanical properties. As a result, the replacing of CIPs by HGPs was proven to be an excellent strategy to improve the dynamic properties of MRPs.

1. Introduction

Magnetorheological plastomer (MRP) is an intelligent magneto-sensitive composite, which is usually composed of magnetically soft particles and a soft polymer [1]. Different from magnetorheological (MR) elastomers [2], the cross-linking density of the polymer matrix for MRP is very low, so the MRP can be easily molded into various shapes and behaves like a solid-like MR gel [3,4]. Meanwhile, the magnetic particles in MRP can move under the action of the magnetic field and the particle structures can be maintained due to the restriction of the matrix after removing the magnetic field. Therefore, the magnetorheological effect of MRP is higher than that of MR elastomers [5,6], and the particle settlement problem is resolved. Therefore, MRPs have important application potential in vibration control [7,8], sensing systems [9,10], and soft robotics [11-13]. In particular, considering the high viscosity of the MRP, it has unique advantages in energy absorption during high-speed impact such as high-speed rail buffer [14,15], weapon brake [16], etc.

Over the past few decades, many studies have shown that the macro mechanical properties of MR materials were closely related to their microstructures [17,18]. As a solid-like gel, the most distinct and important characteristic of MRP is that the particle microstructure can be changed by a magnetic field, so MRPs show the great adjustability of macro properties. Besides, the internal structure of particles can also be changed by adding secondary fillers. Among these fillers, nonmagnetic particles [19] are attractive in MR materials because they can adjust the initial modulus, decrease the density and reduce costs [20]. Interestingly, many exciting results are consulted under exploring the effect of nonmagnetic particles on MR materials. Mitsumata et al found that the magneto-elastic behavior of MR elastomer was enhanced by embedding nonmagnetic particles and they concluded that the enhancement

* Corresponding authors.
E-mail addresses: xuansh@ustc.edu.cn (S. Xuan), gongxl@ustc.edu.cn (X. Gong).

https://doi.org/10.1016/j.jmst.2021.05.075
1005-0302/

was due to the increment of contact between nonmagnetic particles and the particle chain of magnetic particles [21]. Ulicny et al. reported an enhancement in the yield stress of MR fluids caused by the presence of non-magnetizable particles and a three dimensions particle-level simulation was used to explain the results [22]. Rodríguez-Arco et al. also studied the MR properties of a ferrofluid mixed with a diamagnetic microparticle. The results demonstrated the rheological properties were enhanced by dispersing the diamagnetic microparticles [23]. However, the non-magnetic particles also have a negative influence on the mechanical properties. Peng et al. simulated this phenomenon and showed a decrease in the chain length with the addition of non-magnetic particles [24]. Although several attempts have been made in explaining the enhancement effect of nonmagnetic particles, the knowledge about how the nonmagnetic particles affect the structure and mechanical properties of MRPs is not fully understood. At the same time, most of the existing work focuses on viscoelastic properties under shear or the mechanical properties under a quasi-static state [25,26]. As for MRP, it is more suitable for shock-absorbing, so it is also necessary to study the dynamic compressive properties of MRPs under a high strain rate.

The split Hopkinson pressure bar (SHPB) technique is suitable for testing the dynamic properties of MRPs under a high strain rate [27,28]. It can provide dynamic stress-strain curves with a strain rate range of 10^2 to 10^4 [29]. By selecting soft bars and adding pulse shaper [30-32], the mechanical properties of soft materials can be obtained by the existing SHPB technology [33,34]. At the same time, testing the mechanical properties of MRPs at a high strain rate is not only the basis of its application in shock-absorbing but also conducive to the study of the relationship between the macro properties and microstructure. Due to the low cross-linking density of the matrix, the particle structures in MRP will be destroyed and recombined with the deformation. The deformation of the structure in the matrix usually needs several seconds [35]. However, the time scale is about few minutes in quasi-static experiments. In most previous testing, the microstructure changes and the test results are time-dependent. But using SHPB technology, the whole testing process is completed in 100 μs, so there is less recombination process of particles, which is helpful to study the relationship between particle structure and mechanical properties.

In this work, MRPs with different particle structures by controlling the carbonyl iron powder (CIP) and hollow glass powder (HGP) content in the samples were prepared. Then, the dynamic compressive properties of MRP under a high strain rate were tested using the SHPB technology. The mechanical properties of MRP under quasi-static compression were also tested for comparison. To study the relationship between macro mechanical properties and microparticle structure of MRP, the particle structures in MRPs were simulated by a particle-level dynamic method. Then, the effect of non-magnetic particles on the structure and intergranular stress of the MRP was studied. At last, MPRs with 60% particle mass fraction were prepared and their dynamic properties were tested to find the best particle ratio.

2. Experimental

2.1. Materials and preparation

The raw materials of MRP included polypropylene glycol (PPG-1000, Sinopec Group Co. Ltd., China), toluene diisocyanate (TDI, 2,4-TDI at B80%, 2,6-TDI at B20%, Tokyo Chemical Industry Co. Ltd., Japan), Diethylene glycol (DEG, Sinopharm Chemical Reagent Co. Ltd., Shanghai, China), carbonyl iron powder (CIP, type CN, 6 μm average diameter, BASF Aktiengesellschaft, Germany), nonmagnetic hollow glass powder (HGP, type C70, 20 μm average diameter, Fig. S1 in Supporting Information, zhongkehuaxing new materials Co. Ltd, China), and pyrrolidone solvent (Sinopharm Chemical Reagent Co. Ltd., Shanghai, China).

CIPs and HGPs were dispersed in a homemade polyurethane (PU) to prepare MRPs. Firstly, TDI and PPG were added to the flask with a molar ratio of 3:1 at 80°C for 2 h. Then, the reaction temperature was reduced to 40°C, and DEG was added to the reactor. Raised the temperature to 60°C and hold for about 30 min. Thus homemade PU matrix was synthesized. At last, different amounts of CIPs and HGPs were added into PU immediately by vigorously stirring until they were mixed well. The final MRPs with different CIP contents and HGP contents were obtained (Table 1). In addition, 10% pyrrolidone was added to the matrix of the fourth group to better disperse the particles.

2.2. Methods

2.2.1. Quasi-static compression test

An electromechanical universal testing machine (Model 43, MTS System Corporation, China) was used to test the mechanical properties of MRP under quasi-static compression. During the test, two Helmholtz coils were fixed on the gippers of the testing machine to apply a magnetic field and the MRP sample was placed between two Helmholtz coils. The upper coil was controlled to press down at a speed of 1 mm/min and the force and displacement were recorded by the computer. The initial diameter of the sample was 20 mm and the initial height was 3 mm.

2.2.2. Dynamic compression tests of the MRPs

A typical SHPB system equipped with a customized magnetic device was used to test the dynamic mechanical properties of MRPs (Fig. 1(a)). The SHPB system consisted of a striker, an incident bar, a transmission bar, an absorber bar, and an absorber. Two strain gauges were mounted on the incident bar and the transmission bar to measure the incident pulse, the reflected pulse, and the transmitted pulse. A pulse shaper was used between the striker bar and the incident bar to prolong the rising time of the incident pulse. Therefore, the MRP specimen had enough time for stress to reach equilibrium during the experiment. The MRP specimen was placed between the incident bar and the transmission bar and petroleum jelly was used in the interface of the specimen and the bar. The thickness of the sample was 1 mm and the diameter was 13.5 mm. A customized magnetic device was sheathed outside of the sample to provide a uniform magnetic field along the direction of the bar. The magnetic device consisted of three magnetic coils and two iron cores. Fig. 1(b) shows the finite element simulation of magnetic flux density distribution in the magnetic device. The distance between the two coils was 13 mm and a uniform magnetic field was generated between the two coils. The MRP samples lay in the center of two coils, about 6 mm along the symmetric axis, which was long enough to keep the MRP specimen in the experimental region during the loading-unloading process [36]. In this work, a 1 A current was supplied to the coil, and the corresponding magnetic flux density was about 300 mT.

During the test, the striker was driven by the high pressured gas to hit the incident bar and an elastic compressive wave was generated at the impact face. The compressive wave moved forward along the incident bar. When the compressive wave reached the interface of the incident bar and the specimen, due to the difference of wave impedance between the bar and MRP, part of the compressive wave propagates forward through the sample along the transmission rod, and the other part of the compressive wave was reflected back to the incident bar. The incident pulse ε_i, the reflected pulse ε_r, and the transmitted pulse ε_t were measured by the strain gauges on the bars. Fig. 1(c) shows the typical signals measured by the strain gauges mounted on the incident bar

Table 1
Compositions of MRP samples.

Sample no.	Group 1			Group 2		
CIP (vol.%)	3	3	3	6	6	6
HGP (vol.%)	0	9	18	0	9	18
Sample no.	Group 3					
CIP (vol.%)	9	9	9	9	9	
HGP (vol.%)	0	4.5	9	13.5	18	
Sample no.	Group 4					
CIP (wt%)	60	48	36	24	12	
HGP (wt%)	0	12	24	36	48	

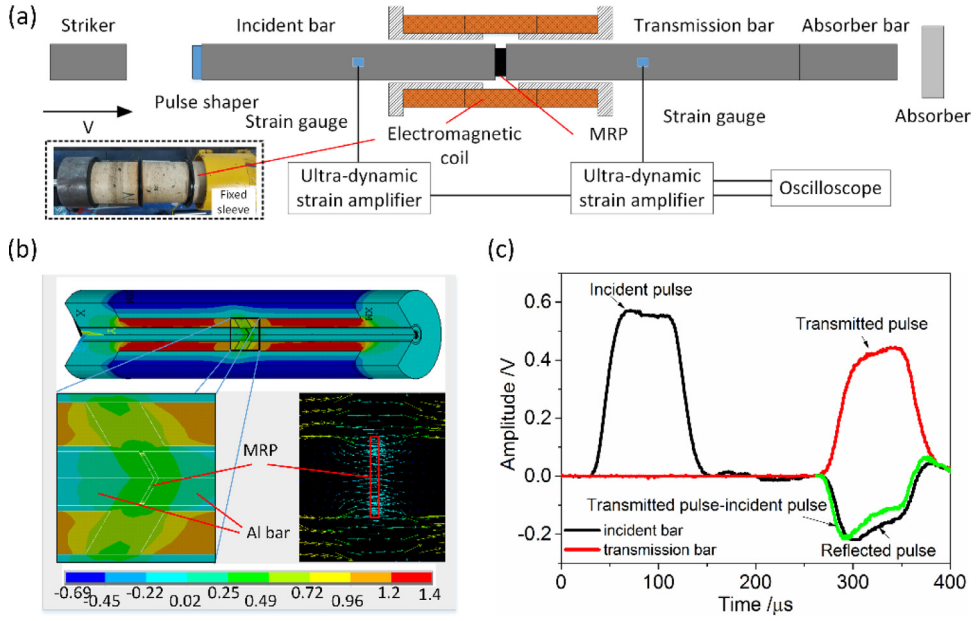

Fig. 1. (a) Schematic illustration of an SHPB system equipped with a customized magnetic device. (b) The finite element simulation of magnetic flux density distribution in the magnetic device. Around the sample, a uniform magnetic field is generated along the direction of the bar. (c) Typical signals measured from the incident bar and the transmission bar in the experiment.

and the transmission bar. As shown in Fig. 1(c), the signals were smooth and the reflected pulse was almost coincident with the transmitted pulse minus the incident pulse, which indicated that it was consistent with the one-dimensional stress wave theory. According to the wave propagation theory, the dynamic stress σ_s, the dynamic strain ε_s, and the strain rate $\dot{\varepsilon}_s$ during the loading-unloading progress can be expressed as:

$$\begin{cases} \sigma_s = \frac{E_b A_b}{A_s}\varepsilon_t \\ \varepsilon_s = -\frac{2C_b}{l_s}\int_0^t \varepsilon_r d\tau \\ \dot{\varepsilon}_s = -\frac{2C_b}{l_s}\varepsilon_r \end{cases} \quad (1)$$

where A_b and A_s are the cross-sectional areas of the bar and the specimen, respectively. E_b is the elastic modulus of the aluminum bar, C_b is the velocity of elastic wave propagation in the bar, and l_s is the thickness of the specimen. Here σ_s and ε_s are the engineering stress and engineering strain, respectively. The true stress σ_t and the true strain ε_t can be obtained by:

$$\begin{cases} \varepsilon_t = ln(1+\varepsilon_s) \\ \sigma_t = (1+\varepsilon_s)\sigma_s \end{cases} \quad (2)$$

3. Particle-level dynamic simulation

The inner particle structures composed of CIPs and HGPs were simulated by a particle-level dynamic method (see Particle-level dynamic simulation, ESI). Once the particle structures are simulated, a compressive strain is applied to the simulation cell to calculate the intergranular stress. During the compression in the experiment, the real strain reaches to 15% in about 100 μs, so the strain is divided into 10000 steps in the simulation, with a 1.5e^{-5} strain increment applied in each step. The time step dt = 0.01 μs. In each time interval, the coordinates of the particle position are corrected according to the strain, and then Eq. (S7) is resolved until the strain reaches the set point. The normal stress is:

$$\sigma_{zz} = \frac{1}{V_c}\sum_{i=1}^{N-1}\sum_{j=i+1}^{N} z_{ij}F_{ij}^z \quad (3)$$

where V_c is the volume of the considered cell, F_{ij}^z represent the component of the total force in the Z direction. In Eq. (3), only the stress between particles is considered, so the stress is called intergranular stress.

4. Results and discussion

Under applying a magnetic field, the CIPs would move due to the dipole force between CIPs. Due to the limitation of the matrix, the inner structure could be preserved after removing the magnetic field. As shown in Fig. 2(a) and Video S1, CIPs formed string-like structures along the direction of the magnetic field, so the mechanical properties of MRP were improved. In Fig. 2(c), the shear storage modulus of MRP with 9 vol.% CIPs increased from 7 kPa to 640 kPa by applying a 960 mT magnetic field. The positions of nonmagnetic HGPs were not directly affected by the magnetic

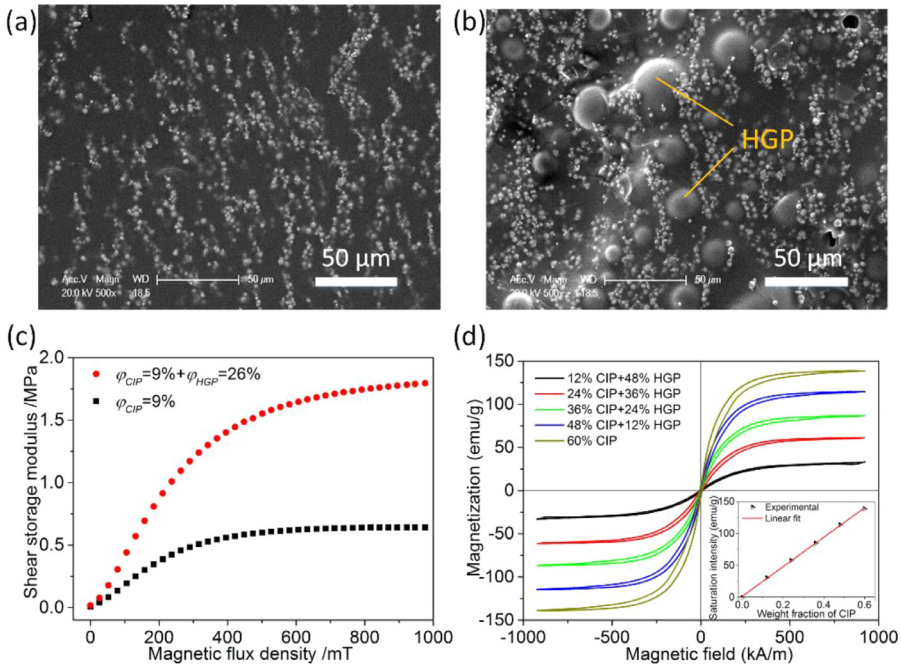

Fig. 2. Scanning electron microscope (SEM) micrographs of MRPs. (a) MRP with 9 vol.% CIPs. (b) MRP with 9 vol.% CIPs and 26 vol.% HGPs. (c) The shear storage modulus of MRP under different magnetic flux densities. (d) Magnetic properties of MRPs with 60 wt% particles.

field and the HGPs were in the gaps of CIP chains (Fig. 2(b)). Here, the average diameters of CIP and HGP were 6 μm and 20 μm, respectively. The diameter of non-magnetic HGPs was much larger than that of magnetic CIPs. When the volume fractions of HGPs were small, the HGPs would be pushed and distribute between the CIP chains. Thus the HGPs not only did not affect the chain-like structure of CIPs but also promoted the formation of a more compact structure with the excluded volume caused by secondary HGPs, which would, in turn, enhance the mechanical properties of MRPs. In Fig. 2(c), under a 960 mT magnetic field, the shear storage modulus of MRP increased from 640 kPa to 1790 kPa by adding 26 vol.% HGPs. Meanwhile, the magnetic properties of MRPs with 60 wt% particles were tested and shown later. The saturated magnetization of MRPs was proportional to the mass fraction of CIPs in the sample, indicating that the adding of HGPs did not affect the magnetic properties of MRPs.

The mechanical properties of MRPs under quasi-static compression were firstly tested on an electromechanical universal testing machine. As shown in Fig. 3(a), the MRP sample was placed between two Helmholtz coil. During the test, a current was applied to the coil to generate a magnetic field and the coils would attract each other under the action of a magnetic field. Therefore, the change of the attractive force between coils with the distance without sample was tested. Then, the attractive force was deducted from the subsequent test results. The stress-strain curves of MRP with different CIP and HGP contents under different magnetic flux densities were shown in Fig. 3. Obviously, with the increase of strain, the increased stress of all samples could be divided into two stages. Firstly, the stress increased rapidly with strain, then yielding at about 1.1%. The difference was that the yield stresses were enhanced by applying a magnetic field. For MRP with 9% CIPs, the yield stress increased from 0.7 kPa to 8.9 kPa. Meanwhile, the yield stresses of MRP were improved by HGPs and the yield stress of MRP with 9% CIPs was increased from 8.9 kPa to 20.0 kPa by adding 18% HGPs. Additionally, the yield process was different with/without a magnetic field. In Fig. 3(a) and (c), the stress always rose with increasing strain, but the growth rate slowed down when the strain was above 1.1%. Under applying a magnetic field (Fig. 3(b) and (d)), the stress would decrease first and then increase near the yield point. Without a magnetic field, CIPs and HPGs were uniformly dispersed in the sample. The yield of samples mainly depended on the properties of the matrix. But when there was a magnetic field, CIPs moved and formed string-like structures along the direction of the magnetic field. During compression, the particle chain may fracture with the deformation of the material, resulting in the reduction of stress.

The dynamic compressive properties of MRPs under different magnetic flux densities and strain rates were tested by a modified SHPB system to understand the overall performance of the MRPs. Figs. 4(a) and S2 show the stress-strain curves and strain rates of MRP under different magnetic fields. Obviously, the dynamic stress increased with increasing magnetic flux density and the MRPs had no obvious yield point when there was no magnetic field. With the increase of the magnetic field, the dynamic stress increased and the inflection point of the curve became more obvious. There was an obvious yield point in the stress-strain curve under a 300 mT magnetic field, which indicated that the chain-like structures were formed in the MRP under this magnetic field. Therefore, a 300 mT magnetic field was applied in the later tests. Fig. 4(b) showed dynamic stress and strain rate changes with strain under a 300 mT magnetic field. During the test, a pulse shaper was used to prolong the rising time of the incident pulse and achieve the dynamic stress equilibrium of the specimen. Therefore, the strain rate had a rising process with the increase of strain. As shown in Fig. 4(b), the strain rate reached the maximum when the strain was less than 2%, which was much smaller than the yield strain of the MRP. So the selection of yield strain was important for investigating the dynamic compressive properties of MRPs.

As polymer composites, the dynamic properties of MRPs were usually dependent on the strain rate. Then, the dynamic properties of MRP under different strain rates loading were tested and the stress increased with increasing of the strain rate. The stress-strain curves in Fig. 4(c) were similar, so the strain rate was controlled at about 2000 s^{-1} in the later tests for easy comparison. The strain rate/strain curves of MRP under different striker velocities were shown in Fig. S3. The strain rates in Fig. 4(c) represented

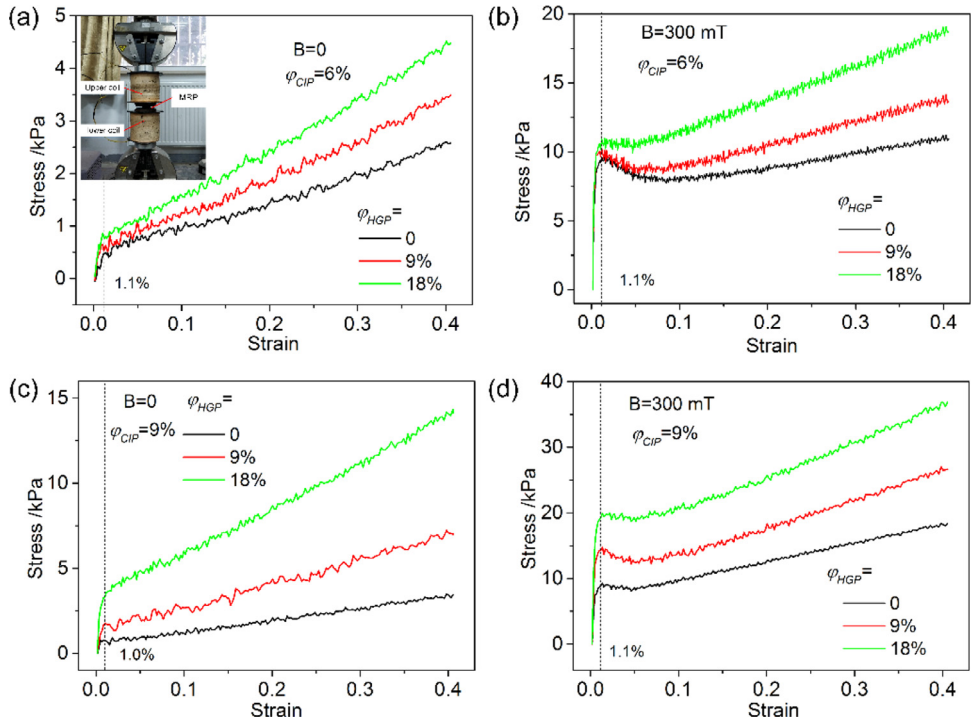

Fig. 3. Stress-strain curves of MRP with different CIP and HGP contents under different magnetic flux densities. (a) φ_{CIP}=6%, 0 mT, (b) φ_{CIP}=6%, 300 mT, (c) φ_{CIP}=9%, 0 mT, (d) φ_{CIP}=9%, 300 mT. Here, the stress and strain were defined as positive when the sample was pressed.

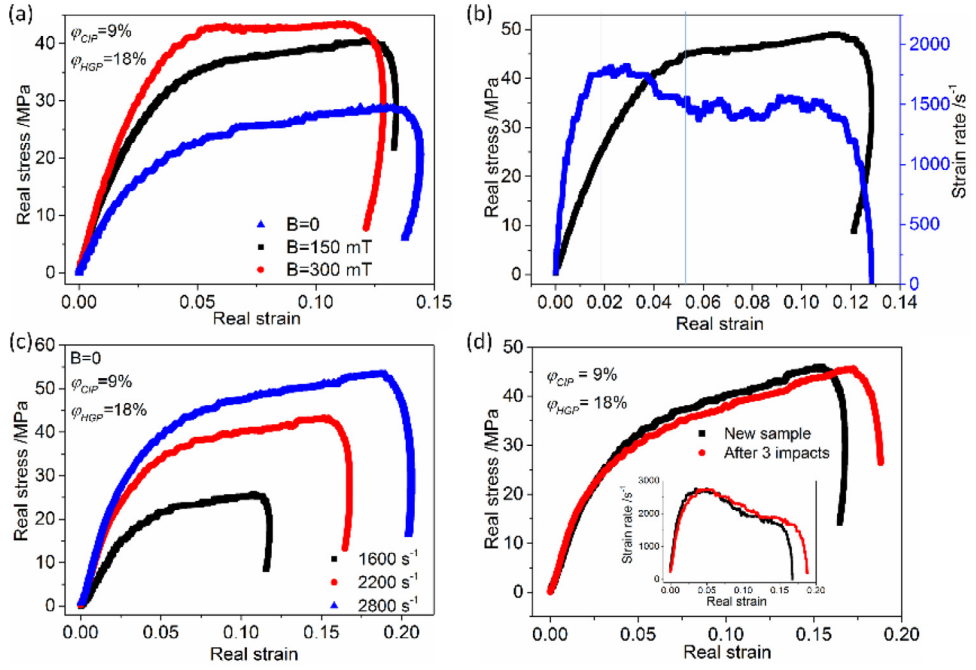

Fig. 4. Dynamic compressive properties of MRP with 9 vol.% CIPs and 18 vol.% HGPs. (a) Stress/strain curves under different magnetic flux densities. (b) Dynamic stress and strain rate of MRP under a 300 mT magnetic field. (c) Stress/strain curves of MRP at different strain rates. The strain rates in the figure represent the maximum strain rates. (d) Stress/strain curves of MRP before and after three impacts.

the maximum strain rates during the compression. Meanwhile, the dynamic properties of MRP with 9 vol.% CIPs and 18 vol.% HGPs before and after three impacts were tested and the stress-strain curves were shown in Fig. 4(d). The stress curves in the figure basically coincided, indicating that the repeatability of the MRP was good and the impact did not damage the HGPs in MRP.

The dynamic compressive properties of MRPs with different HGPs were shown in Fig. 5(a) and (b). Obviously, the dynamic stress increased with increasing HGP content. Similar to the quasi-static test, the MRPs had no obvious yield point when there was no magnetic field. The difference was that the yield strain increased. Here the yield point was determined by the intersection of two straight lines for the convenience of comparison. Similarly, the yield strain of MRPs under a magnetic field increased (4%-5%), which was caused by the viscoelastic properties of the polymer matrix. The state of the polymer matrix changed from a viscoelas-

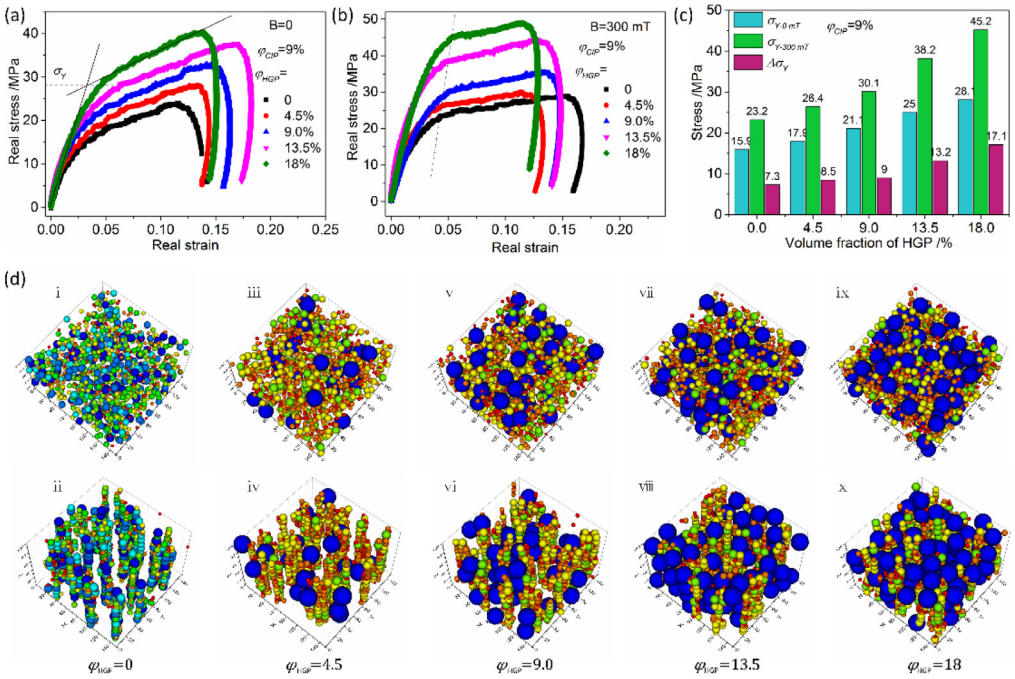

Fig. 5. Dynamic compressive stress/strain curves of MRPs with 9 vol% CIPs and different HGPs under different magnetic flux densities. (a) B=0, (b) B=300 mT. (c) Yield stresses under different magnetic fields and magnetic-induced yield stresses of MRPs with different HGP contents. (d) Simulated results of particle structures in MRPs with different HGPs before and after applying a magnetic field. The blue balls represent the HGPs. The direction of the magnetic field is along the Z-axis.

tic state to a rubber-like state with the increase of strain rate and the yield strain increased. In addition, another difference from the quasi-static experimental results was that the stress of MRP did not decrease significantly near the yield point under a magnetic field. It meant that the particle structure was more stable under high strain rate loading. On the one hand, the binding effect of the matrix was enhanced due to the transition of the matrix state. On the other hand, the compression process was fast ($<$100 μs) and the particle structure had little to change near the yield point. As a result, the stress did not decrease.

Since the MRPs would be mostly used in shock absorption, the yield stress of MRP was an important parameter. To better analyze the effect of HGPs on the dynamic mechanical properties of MRPs, yield stresses under different magnetic fields and the magnetic-induced yield stresses of MRPs as a function of volume fraction of HGPs were summarized (Fig. 5(c)). Here, the magnetic-induced yield stress $\Delta\sigma_Y$ was the yield stress under a magnetic field $\sigma_{Y-300mT}$ minus the initial yield stress σ_{Y-0mT} without a magnetic field. The yield stresses with/without a magnetic field increased with increasing HGP content. As a secondary filler, the modulus of HGP was much larger than that of the matrix. The mechanical properties of MRPs were enhanced by HGPs as reinforcing particles. In our case, non-magnetic particles had little effect on the magnetic-induced properties of MR materials because the adding of HGPs did not affect the magnetic properties of MRPs (Fig. S4). But for MRPs with 9 vol.% CIPs, the magnetic-induced yield stress was enhanced by adding 18 vol.% HGPs and $\Delta\sigma_Y$ increased from 7.3 MPa to 17.1 MPa (234%). Combined with the simulated results in Fig. 5(d), it could be found that CIPs formed chain-like structures along the direction of the magnetic field. With the increase of HGP content, the volume fraction of CIPs in the matrix was increased and more compact CIP structures were formed with the excluded volume caused by secondary HGPs. Meanwhile, HGPs were distributed among the CIP chains, which strengthened the interaction between the CIP chains and further improved the magnetic-induced yield stress of the MRP.

The intergranular stresses in MRPs were further calculated to analyze the enhanced effect of HGPs on dynamic compressive properties. Fig. 6(a) and (b) shows the calculated intergranular stresses in MRPs with 9 vol.% CIPs and different HGP contents under compression with and without a magnetic field, respectively. Without a magnetic field, CIPs and HGPs were uniformly dispersed in the matrix. During compression, the distance between particles decreased. When the strain reached about 7%, the particles began to contact and the stress between particles rose rapidly. The stress increased with the increasing HGP content but the intergranular stress at 15% strain was less than 0.5 MPa, indicating that the enhancement of yield stress was independent of the direct contact stress between particles when there was not a magnetic field. The increased yield stress of MRP was due to the that the proportion of hard phase in MRP increased with increasing HGP content, which could enhance the properties of a particle-reinforced composite.

As shown in Fig. 6(d) and (e), CIPs formed chain-like structures along the direction of the magnetic field. Most of the particles were pushed by CIPs and distributed between the CIP chains, and some HGPs broke the CIP chains and interpenetrated on one CIP chain. There were also some CIPs formed short chains between two HGPs. Therefore, CIPs and HGPs formed a three-dimensional structure along the direction of the magnetic field. Under compression, the particle structure itself could also resist deformation and produce normal stress. As shown in Fig. 6(b), the intergranular stresses first increased and then yielded at about 5% strain with the increase of strain. When the particle structure was squeezed, the compressive stress was produced between the particles. With the increase of compressive strain, the CIP chains buckled and the particle structure yielded, which resulted in a significant yield point in the intergranular stress. This was also the reason why there was an obvious yield point in the dynamic stress-strain curves under applying a magnetic field in Fig. 5(b). With the increase of HGP content, the slope at the beginning of the curve increased slightly. This was because the volume fraction of CIPs increased from 9% to 11% with the excluded volume caused

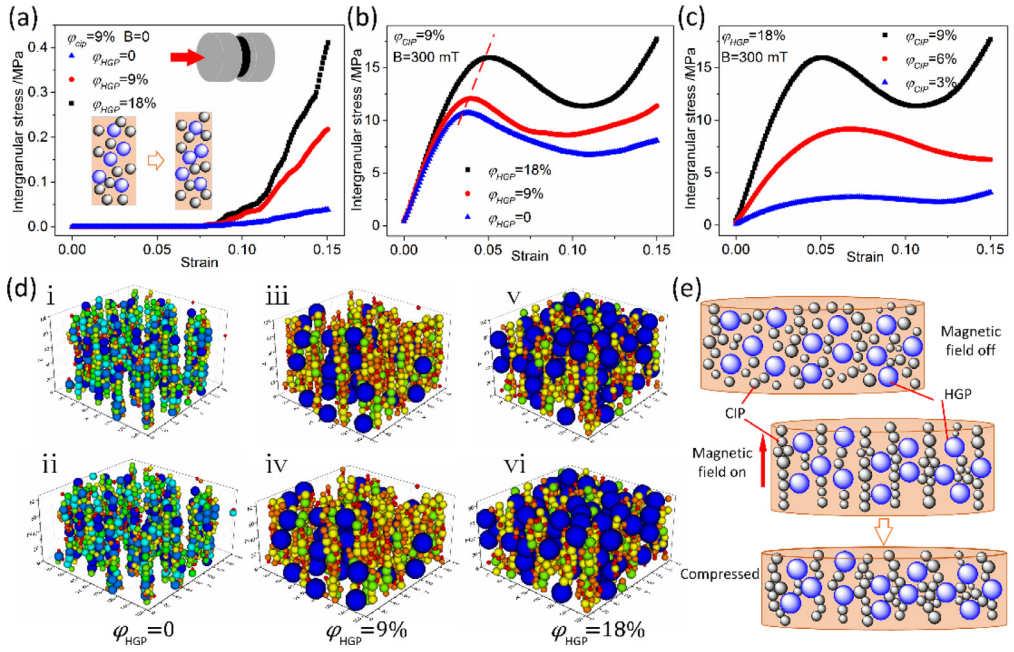

Fig. 6. Calculated intergranular stresses in MRPs with 9 vol% CIPs and different HGP contents under compression. (a) B=0 mT and (b) B=300 mT. (c) Calculated intergranular stresses in MRPs with 18 vol.% HGPs and different CIP contents. (d) Simulated particle structures in MRPs with 9 vol.% CIPs and different HGP contents before (i, iii, v) and after compression (ii, iv, vi). The compressive strain is 15%. (e) Schematic diagram of internal particle structures of MRP in different states.

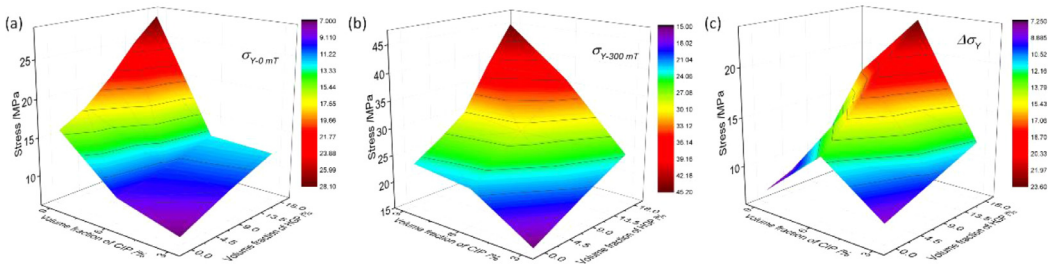

Fig. 7. Yield stresses (a) without a magnetic field, (b) under a 300 mT magnetic field, and (c) magnetic-induced yield stresses of MRPs with different CIPs and HGPs.

by secondary HGPs. At the same time, the yield of intergranular stresses and strains also increased with increasing HGP content, corresponding to the results in Fig. 5(b). As shown in Fig. 6(e), during compression, the HGPs between the CIP chains could help to resist deformation, thereby increasing the yield strain and stress. As for the intergranular stresses in MRPs with different CIP contents in Fig. 6(c), the slope at the beginning of the curve increased with increasing CIP content. Meanwhile, the yield strain slightly increased with decreased CIP content because the ratio of HGPs to CIPs increased. In addition, the shape of the intergranular stress-strain curves was different from that of the experimental results. Here, both the contribution of the matrix and the effect of the strain rate change were not considered.

The dynamic compressive properties of MRPs with 3 vol.% CIP (Fig. S5) and 6 vol.% CIP (Fig. S6) were also tested and the yield stresses σ_{Y-0mT}, $\sigma_{Y-300mT}$, and $\Delta\sigma_Y$ of three groups of MRPs were shown in Fig. 7. Firstly, it should be pointed out that, for MRPs with 3 vol.% CIP and 6 vol.% CIP, there was a decrease of stress near the yield point (Figs. S5(b) and S6(b)), which was different from the results in Fig. 5(b). Here, the trend of yield stresses was similar to that in Fig. 5. The stress surfaces in Fig. 7(a) and (b) were plains growing in one direction, indicating that the yield stress of the MRP could be continuously adjusted within the range by controlling the particle content. Through further comparison, it could be found that σ_{Y-0mT} and $\sigma_{Y-300mT}$ of MRP with 3% CIPs and 18% HPGs (12.3 MPa and 24.3 MPa) were larger than that of MRP with 6% CIPs (9.3 MPa and 21.9 MPa) without HGPs. Therefore, the same mechanical properties could be achieved by replacing some CIPs with less dense and cheaper HGPs.

By keeping HGP content as a constant, MRPs with 6% CIPs had the largest $\Delta\sigma_Y$ (Fig. 7(c)). By comparing the particle structures in Figs. 5(d), S5(d) and S6(d), it could be seen that the CIP structures in MRPs with 9% CIPs were dense, which led to a larger σ_{Y-0mT} and the effect of HGPs was not obvious, while the CIP structures in MRPs with 3% CIPs were sparse and they had less coordination with HGPs. So MRPs with 6% CIPs had the largest $\Delta\sigma_Y$. The decrease of stress near the yield point for MRP with 6% CIPs also indicated that the interaction between HGPs and CIP chains was the most. At the same time, the relative magnetorheological effect was important in engineering applications. With increasing HGP contents, the relative MR effect under dynamic compression ($\Delta\sigma_Y/\sigma_{Y-0mT}$) were changed from 0.46 to 0.61 for MRPs with 9% CIP, 1.35 to 1.86 for MRPs with 6% CIP, and 1.14 to 0.98 for MRPs with 3% CIP. MRPs with 6% CIPs also had the largest MR effects.

At last, MRPs with 60 wt% fillers were prepared and the dynamic compressive properties were shown in Fig. 8(a) and (b). The volume ratio of CIPs to HGPs in this group of MRPs varies in a large range. With the decrease of CIP content, the volume fraction of CIP is 17%, 10%, 6.3%, 3.5%, and 1.5%, and the volume fraction of HGP is 0, 26%, 42%, 53%, and 61%, respectively. It could be found that HGPs still had an enhancement effect in a large particle proportion range. However, when the mass ratio of HGP to

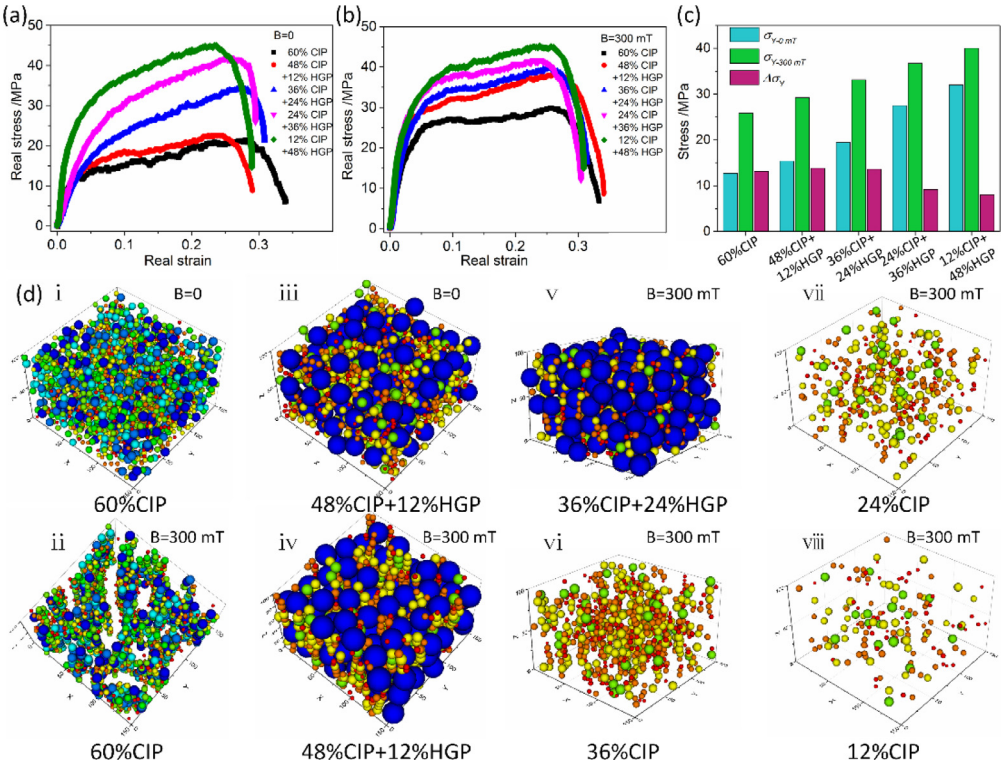

Fig. 8. Dynamic compressive stress-strain curves of MRP with 60 wt% fillers under different magnetic flux densities. (a) *B*=0, (b) *B*=300 mT. (c) Yield stresses under different magnetic fields and magnetic-induced yield stresses of MRPs as a function of volume fraction of HGPs. (d) Simulated results of particle structures in MRPs before and after applying a magnetic field. The big blue balls represent the HGPs. The direction of the magnetic field is along the *Z*-axis. In image vi-viii, only CIPs are shown for convenience of observation.

CIP was greater than 0.67, the enhancement effect was not obvious and even reduced the magnetic-induced yield stress. In particular, only the $\Delta\sigma_Y$ of MRP with 48 wt% CIP and 12 wt% HGP increased slightly and $\Delta\sigma_Y$ decreased with the further increase of HGPs. As shown in Fig. 8(d), when the content of HGPs was too high, the CIPs were distributed in isolated regions segregated by HGPs. In Fig. 8(d) v and vi, the CIPs could only form a short cluster structure. With the further increase of HGP content, the CIPs showed uniform distribution in the matrix and could not form long-chain structures, so the $\Delta\sigma_Y$ was decreased by adding of HGPs. Although the content of HGPs could not be too high, for MRP with 48 wt% CIP and 12% HGP, due to the small density of HGPs (0.73 g/cm^3), the overall density of MRP decreased from 2.1 g/cm^3 to 1.6 g/cm^3. So, a higher specific modulus could be achieved by replacing some CIPs with HGPs, which was beneficial to practical applications.

5. Conclusion

In this work, the dynamic compressive properties of the HGPs enhanced MRPs under high strain rate were tested using the modified SHPB technology. The results showed that the HGPs could greatly improve the yield stress of the MRP without changing the yield strain of the MRP. In particular, the magnetically induced yield stress of MRP with 9 vol.% CIPs increased from 7.3 MPa to 17.1 MPa by adding 18 vol.% HGPs. To study the effect of HGPs on the structure and mechanical properties of MRPs, the inner particle structures of MRPs were further simulated and the intergranular stresses were calculated by a particle-level dynamic method. Combined with the simulation results, it was concluded that there were two reasons for the enhancement of magneto-mechanical properties by non-magnetic HGPs. On the one hand, the volume fraction of CIPs in the matrix was increased with the excluded volume caused by secondary HGPs; on the other hand, HGPs distributed among the CIP chains and strengthened the interaction between the CIP chains, which enhanced the stability of particle structure and in turn improved the yield stress. In addition, excessive HGPs would weaken the enhancement effect of HGPs and even reduced the magneto-mechanical properties of MRPs. When the content of HGPs was larger than 42 vol.%, CIPs were separated in isolated regions and could not form long-chain structures. Based on the above analysis, better performance of MRP could be achieved by replacing some CIPs with HGPs in practical application.

Declaration of Competing Interest

The authors report no declarations of interest.

Acknowledgements

This work was financially supported by the National Natural Science Foundation of China (Nos. 12102424, 12132016, 11972343, and 11822209), the National Key R&D Program of China (No. 2018YFB1201703), the Anhui's Key R&D Program of China (No. 202104a05020009), and the Strategic Priority Research Program of the Chinese Academy of Sciences (No. XDB22040502).

Supplementary materials

Supplementary material associated with this article can be found, in the online version, at doi:10.1016/j.jmst.2021.05.075.

References

[1] Y.G. Xu, X.L. Gong, S.H. Xuan, W. Zhang, Y.C. Fan, Soft Matter 7 (2011) 5246–5254.
[2] A.K. Bastola, M. Hossain, Compos. B-Eng. 200 (2020) 108348.
[3] A.Y. Zubarev, D.N. Chirikov, D.Y. Borin, G.V. Stepanov, Soft Matter 12 (2016) 6473–6480.

[4] P.G. Yang, M. Yu, H.P. Luo, J. Fu, H. Qu, Y.P. Xie, Appl. Surf. Sci. 416 (2017) 772–780.
[5] M. Yu, S. Qi, J. Fu, M. Zhu, D. Chen, Compos. Sci. Technol. 139 (2017) 36–46.
[6] A. Dargahi, R. Sedaghati, S. Rakheja, Compos. B-Eng. 159 (2019) 269–283.
[7] S. Kaluvan, V. Thirumavalavan, S. Kim, S.B. Choi, Sens. Actuat. A 239 (2016) 166–173.
[8] S.B. Choi, W.H. Li, M. Yu, H.P. Du, J. Fu, P.X. Do, Smart Mater. Struct. 25 (2016) 043001.
[9] L. Ding, S.H. Xuan, J.B. Feng, X.L. Gong, Composer Part A-Appl. Sci. 100 (2017) 97–105.
[10] J.Q. Xu, L. Pei, J. Li, H.M. Pang, Z.Y. Li, B.S. Li, S.H. Xuan, X.L. Gong, Compos. Sci. Technol. 183 (2019) 107820.
[11] A. Alkhalaf, A. Hooshiar, J. Dargahi, Compos. B-Eng. 190 (2020) 107888.
[12] X. Yuan, X.F. Zhou, Y.D. Liang, L.J. Wang, R.M. Chen, M.Y. Zhang, H.Y. Pu, S.H. Xuan, J.B. Wu, W.J. Wen, Compos. B-Eng. 193 (2020) 107988.
[13] P. Testa, R.W. Style, J.Z. Cui, C. Donnelly, E. Borisova, P.M. Derlet, E.R. Dufresne, L.J. Heyderman, Adv. Mater. 31 (2019) 1900561.
[14] H.M. Pang, S.H. Xuan, C.L. Sun, X.L. Gong, Smart Mater. Struct. 26 (2017) 105017.
[15] H.K. Kim, H.S. Kim, Y.K. Kim, Smart Mater. Struct. 26 (2017) 015016.
[16] Z.C. Li, Y. Gong, J. Wang, J. Intell. Mater. Syst. Struct. 30 (2019) 677–688.
[17] Y.L. Qiao, J.T. Zhang, M. Zhang, L.S. Liu, P.C. Zhai, Compos. Sci. Technol. 204 (2021) 108637.
[18] K. Danas, J. Mech. Phys. Solids 105 (2017) 25–53.
[19] L.L. Fan, G.P. Wang, W.J. Wang, H.L. Lu, F.F. Yang, X.T. Rui, J. Mater. Sci. 54 (2019) 1326–1340.
[20] S.R. Khimi, K.L. Pickering, Compos. B-Eng. 90 (2016) 115–125.
[21] T. Mitsumata, S. Ohori, N. Chiba, M. Kawai, Soft Matter 9 (2013) 10108–10116.
[22] J.C. Ulicny, K.S. Snavely, M.A. Golden, D.J. Klingenberg, Appl. Phys. Lett. 96 (2010) 231903.
[23] L. Rodriguez-Arco, M.T. Lopez-Lopez, A.Y. Zubarev, K. Gdula, J.D.G. Duran, Soft Matter 10 (2014) 6256–6265.
[24] X.L. Peng, Y. Min, T.Y. Ma, W. Luo, M. Yan, J. Magn. Magn. Mater. 321 (2009) 1221–1226.
[25] K. Nagashima, S. Kanauchi, M. Kawai, T. Mitsumata, S. Tamesue, T. Yamauchi, J. Appl. Phys. 118 (2015) 024903.
[26] Y.G. Xu, X.L. Gong, T.X. Liu, S.H. Xuan, J. Rheol. 58 (2014) 659–679.
[27] Z.H. Song, Z.H. Wang, H.W. Ma, H.J. Xuan, Compos. B-Eng. 60 (2014) 531–536.
[28] M. Tarfaoui, S. Choukri, A. Neme, Compos. Sci. Technol. 68 (2008) 477–485.
[29] Z.M. Jia, D. Hui, G.Q. Yuan, J. Lair, K.T. Lau, F.J. Xu, Compos. B-Eng. 105 (2016) 132–137.
[30] J. Xu, Y.B. Li, D.Y. Ge, B.H. Liu, M.Y. Zhu, Int. J. Impact Eng. 38 (2011) 106–114.
[31] B. Song, W. Chen, J. Eng. Mater. Technol. 125 (2003) 294–301.
[32] J.Q. Xu, P.F. Wang, H.M. Pang, Y.P. Wang, J. Wu, S.H. Xuan, X.L. Gong, Compos. Sci. Technol. 159 (2018) 50–58.
[33] Y.P. Wang, S. Wang, C.H. Xu, S.H. Xuan, W.Q. Jiang, X.L. Gong, Compos. Sci. Technol. 127 (2016) 169–176.
[34] J.T. Fan, J. Weerheijm, L.J. Sluys, Compos. Sci. Technol. 118 (2015) 55–62.
[35] T.X. Liu, X.L. Gong, Y.G. Xu, S.H. Xuan, W.Q. Jiang, Soft Matter 9 (2013) 10069–10080.
[36] G.J. Liao, X.L. Gong, S.H. Xuan, Ind. Eng. Chem. Res. 52 (2013) 8445–8453.